Global Multimodel Analysis of Drought in Runoff for the Second Half of the Twentieth Century

M. H. J. VAN HUIJGEVOORT,* P. HAZENBERG,*,+ H. A. J. VAN LANEN,* A. J. TEULING,* D. B. CLARK,# S. FOLWELL,# S. N. GOSLING,@ N. HANASAKI,& J. HEINKE,** S. KOIRALA,++ T. STACKE,## F. VOSS,@@ J. SHEFFIELD,&& AND R. UIJLENHOET*

* *Hydrology and Quantitative Water Management Group, Wageningen University, Wageningen, Netherlands*
# *Centre for Ecology and Hydrology, Wallingford, United Kingdom*
@ *School of Geography, University of Nottingham, Nottingham, United Kingdom*
& *National Institute for Environmental Studies, Tsukuba, Japan*
** *Potsdam Institute for Climate Impact Research, Potsdam, Germany, and International Livestock Research Institute, Nairobi, Kenya*
++ *Institute of Engineering Innovation, University of Tokyo, Tokyo, Japan*
Terrestrial Hydrology Group, Max Planck Institute for Meteorology, Hamburg, Germany
@@ *Center for Environmental Systems Research, University of Kassel, Kassel, Germany*
&& *Department of Civil and Environmental Engineering, Princeton University, Princeton, New Jersey*

(Manuscript received 18 December 2012, in final form 22 May 2013)

ABSTRACT

During the past decades large-scale models have been developed to simulate global and continental terrestrial water cycles. It is an open question whether these models are suitable to capture hydrological drought, in terms of runoff, on a global scale. A multimodel ensemble analysis was carried out to evaluate if 10 such large-scale models agree on major drought events during the second half of the twentieth century. Time series of monthly precipitation, monthly total runoff from 10 global hydrological models, and their ensemble median have been used to identify drought. Temporal development of area in drought for various regions across the globe was investigated. Model spread was largest in regions with low runoff and smallest in regions with high runoff. In vast regions, correlation between runoff drought derived from the models and meteorological drought was found to be low. This indicated that models add information to the signal derived from precipitation and that runoff drought cannot directly be determined from precipitation data alone in global drought analyses with a constant aggregation period. However, duration and spatial extent of major drought events differed between models. Some models showed a fast runoff response to rainfall, which led to deviations from reported drought events in slowly responding hydrological systems. By using an ensemble of models, this fast runoff response was partly overcome and delay in drought propagating from meteorological drought to drought in runoff was included. Finally, an ensemble of models also allows for consideration of uncertainty associated with individual model structures.

1. Introduction

Drought is a natural hazard that occurs at the land surface all over the world and can have large economic, social, and environmental impacts (Wilhite 2000). Drought is defined as a period of below-average natural water availability caused by low precipitation and/or high evaporation rates. It is characterized as a deviation from normal conditions of the physical system (climate and hydrology), which is reflected in variables such as precipitation, soil moisture, groundwater, and streamflow (Tallaksen and van Lanen 2004; Wilhite 2000). Dry areas worldwide have been expanding in recent decades and are expected to continue to do so in the near future (Dai 2011; Romm 2011; Fraser et al. 2013), leading to more severe impacts of drought events. In the twenty-first century, drought may intensify in parts of Europe, central North America, Central America and Mexico,

Denotes Open Access content.

+ Current affiliation: Department of Atmospheric Sciences, University of Arizona, Tucson, Arizona.

Corresponding author address: Marjolein van Huijgevoort, Wageningen University, P.O. Box 47, 6700 AA, Wageningen, Netherlands.
E-mail: marjolein.vanhuijgevoort@wur.nl

DOI: 10.1175/JHM-D-12-0186.1

northeast Brazil, and southern Africa (Seneviratne et al. 2012). To reduce impacts of drought, thorough knowledge regarding its space–time development both for the current and future climates is essential.

Long time series of hydrometeorological variables are needed for drought analysis. At the global scale, observed time series are usually not available. Instead, large-scale models can be used to simulate global and continental terrestrial water cycles. In principle, results from large-scale models offer possibilities for hydrological drought analyses (drought in runoff), although certain limitations are expected, depending on the model and data used. For example, any given model is unlikely to be able to accurately simulate runoff for all regions of the globe, the models used in this study are typically run at 0.5° resolution, and model performance/ability is somewhat contingent upon the quality of the input data that are used for calibrating, validating, or forcing the model.

To reduce the influence caused by a single-model structure, multimodel drought analyses provide a promising way forward. Results of 11 global models were used in the Water Model Intercomparison Project (WaterMIP). Haddeland et al. (2011) investigated whether land surface models and global hydrological models showed consistent differences in their simulations of the water cycle by looking at the hydrological regimes (e.g., mean monthly values) compared to observations and global statistics. They concluded that ''the models gave a large range in global and regional water flux and storage terms.'' No clear differences were found between the two groups of models. Because of uncertainty caused by the differences between model results, Haddeland et al. (2011) recommend using multiple models instead of a single model realization when studying climate change impacts. However, it has not yet been determined whether multimodel analyses provide suitable data for the analysis of global hydrological extremes, such as drought.

Sheffield et al. (2009) used a single large-scale model, Variable Infiltration Capacity (VIC), to simulate soil moisture globally. From simulated series, they calculated soil moisture drought characteristics and investigated the spatial extent of soil moisture droughts over the globe. Andreadis et al. (2005) also employed the VIC model to simulate time series of soil moisture and runoff and studied associated drought over the continental United States, which was extended to a multimodel analysis by Wang et al. (2009). Wang et al. (2011) examined large-scale soil moisture drought events and trends for China using a similar set of models. In a global study, Corzo Perez et al. (2011) investigated results of hydrological drought approaches with the global hydrological model WaterGAP. However, a spatiotemporal characterization of global hydrological drought (e.g., runoff and streamflow) from a multimodel ensemble is lacking.

Multimodel studies have been carried out for Europe by Prudhomme et al. (2011), Gudmundsson et al. (2012a,b), and Stahl et al. (2012). Prudhomme et al. (2011) assessed the ability of three global, gridded hydrological models to simulate large-scale high- and low-flow events in a comparison with catalogues of historical droughts and high flows derived from discharge observations across Europe. According to Prudhomme et al. (2011) there was a reasonable similarity between observed and simulated drought, while it was recommended that differences between the various model outputs and observations should be taken into account in further studies. They also concluded that ''model behavior and the ability to reproduce hydrological processes may be very different in different climate regimes'' (Prudhomme et al. 2011, p. 1202). Gudmundsson et al. (2012a,b) compared an ensemble of nine large-scale hydrological models to observed discharge for small catchments in Europe to quantify the uncertainty in model simulations. One of their main conclusions was that, despite the large spread in model performance, ''the ensemble mean is a pragmatic and reliable estimator of spatially aggregated time series of annual low, mean and high flows across Europe'' (Gudmundsson et al. 2012a, p. 604). The main objective of Stahl et al. (2012) was to assess the accuracy of a multimodel ensemble of eight large-scale models by comparing modeled trends against trends in observed streamflow in Europe. Results showed that individual models disagreed regarding magnitudes and even trend direction in several areas (Stahl et al. 2012). They also found that variability in the simulated trends was high and encouraged multimodel approaches and similar studies for other continents.

Another issue concerning the analysis of hydrological drought at the global scale is the lack of reliable, observed data to test model results. At the global scale, validation against hydrological observations (river flow) is difficult, because (i) only a limited number of measurements exist and (ii) observed river flow at gauging stations cannot be compared directly to gridded runoff (i.e., natural large basins and a routing approach needed). Instead, the present study looks for agreement between an ensemble of models as an indication that results are plausible and compares drought in model results with meteorological drought to identify information added by the large-scale models, which is expected to occur because of the nonlinear transformation of meteorological drought in the subsurface.

The aim of this study is to investigate whether large-scale models are able to reproduce hydrological drought (runoff), to identify the variability among models in different climate zones, and to analyze the differences between meteorological and hydrological drought. This was done by

TABLE 1. Main characteristics of the selected models (derived from Haddeland et al. 2011). The model names in the first column are GWAVA = Global Water Availability Assessment; HTESSEL = Hydrology-Tiled ECMWF Scheme for Surface Exchange over Land; JULES = Joint UK Land Environment Simulator; LPJmL = Lund–Potsdam–Jena Managed Land Dynamic Global Vegetation and Water Balance; Mac-PDM = Macro-Scale Probability-Distributed Moisture; MATSIRO = Minimal Advanced Treatments of Surface Integration and Runoff; MPI-HM = Max Planck Institute Hydrology Model; ORCHIDEE = Organising Carbon and Hydrology in Dynamic Ecosystems; WaterGAP = Water Global Analysis and Prognosis.

Model name	Model time step	Meteorological forcing variables[a]	Energy balance	Evapotranspiration scheme[b]	Runoff scheme[c]	Snow scheme	Reference(s)
GWAVA	Daily	*P*, *T*, *W*, *Q*, LWn, SW, SP	No	Penman– Monteith	Saturation excess/beta function	Degree day	Meigh et al. (1999)
H08	6 h	*R*, *S*, *T*, *W*, *Q*, LW, SW, SP	Yes	Bulk formula	Saturation excess/beta function	Energy balance	Hanasaki et al. (2008)
HTESSEL	1 h	*R*, *S*, *T*, *W*, *Q*, LW, SW, SP	Yes	Penman– Monteith	VIC/Darcy	Energy balance	Balsamo et al. (2009)
JULES	1 h	*R*, *S*, *T*, *W*, *Q*, LW, SW, SP	Yes	Penman– Monteith	Infiltration excess/Darcy	Energy balance	Best et al. (2011); Clark et al. (2011)
LPJmL	Daily	*P*, *T*, LWn, SW	No	Priestley– Taylor	Saturation excess	Degree day	Bondeau et al. (2007); Rost et al. (2008)
Mac-PDM	Daily	*P*, *T*, *W*, *Q*, LWn, SW	No	Penman– Monteith	Saturation excess/beta function	Degree day	Arnell (1999); Gosling and Arnell (2011)
MATSIRO	1 h	*R*, *S*, *T*, *W*, *Q*, LW, SW, SP	Yes	Bulk formula	Infiltration and saturation excess/ groundwater	Energy balance	Takata et al. (2003); Koirala (2010)
MPI-HM	Daily	*P*, *T*	No	Thornthwaite	Saturation excess/ beta function	Degree day	Hagemann and Gates (2003); Hagemann and Dümenil (1997)
ORCHIDEE	15 min	*R*, *S*, *T*, *W*, *Q*, SW, LW, SP	Yes	Bulk formula	Saturation excess	Energy balance	de Rosnay and Polcher (1998)
WaterGAP	Daily	*P*, *T*, LWn, SW	No	Priestley– Taylor	Beta function	Degree day	Alcamo et al. (2003)

[a] *R*, rainfall rate; *S*, snowfall rate; *P*, precipitation (rain or snow distinguished in the model); *T*, air temperature; *W*, wind speed; *Q*, specific humidity; LW, longwave radiation flux (downward); LWn, longwave radiation flux (net); SW, shortwave radiation flux (downward), SP, surface pressure.

[b] Bulk formula is when bulk transfer coefficients are used when calculating the turbulent heat fluxes.

[c] Beta function is when runoff is a nonlinear function of soil moisture.

a global, multimodel analysis of drought based on monthly aggregated runoff data from 10 different models, the ensemble median of these models, and global precipitation data. Patterns and occurrence of drought characteristics corresponding to the ensemble median are investigated, while taking into account the variability among individual models. Differences between precipitation droughts and runoff droughts derived from the ensemble median are identified. This study aims to contribute to our knowledge of the potential of large-scale models to capture extreme hydrological drought events, both in space and in time.

2. Large-scale models

Through the project Water and Global Change (WATCH; www.eu-watch.org), results from different large-scale models using the same forcing data were made available. The multimodel analysis in the current paper comprises 10 models: H08, HTessel, JULES, ORCHIDEE, MATSIRO, WaterGAP, MPI-HM, LPJml, GWAVA, and Mac-PDM. A condensed overview with characteristics of each model, after Haddeland et al. (2011), is presented in Table 1. The model ensemble median and variability between the models were derived to represent the overall hydrological behavior rather than focusing on individual models. This study does not intend to evaluate individual models.

The use of an ensemble mean is quite common when analyzing large-scale model output, for both soil moisture and runoff (e.g., Haddeland et al. 2011; Gudmundsson et al. 2012a; Stahl et al. 2012), and is often found to be closer to the observations than results of individual

models (Gao and Dirmeyer 2006; Guo et al. 2007). Tallaksen et al. (2011) found that the ensemble median performed better in comparison against observations than the ensemble mean. Wang et al. (2011) also use an ensemble median to exclude the effect of outliers. In this study, we have chosen to use the multimodel ensemble median rather than the mean because of zero runoff periods in dry regions. In these cases, the ensemble median gives a more robust result compared to the ensemble mean. A minimum threshold of $10^{-6}\,\mathrm{kg\,m^{-2}\,s^{-1}}$ was used to avoid infinitesimally small values of runoff, which may occur in the model output. All values below this threshold have been set to zero.

All models had the same simulation setup and forcing data described in detail in Haddeland et al. (2011) and Gudmundsson et al. (2012a), but the employed time step, meteorological variables, and model structure differ between the models (Table 1). They used the land mask defined by the Climate Research Unit (CRU) at a resolution of 0.5° × 0.5°. Only land points (67 420 grid cells in total) were considered by the models. Model forcing was provided by the WATCH forcing data (WFD) developed by Weedon et al. (2011). The WFD consist of gridded time series of meteorological variables (e.g., rainfall, snowfall, temperature, and wind speed) both on a subdaily and daily basis for 1958–2001 with a resolution of 0.5° × 0.5°. The WFD originate from modification (bias correction and downscaling) of the 40-yr European Centre for Medium-Range Weather Forecasts (ECMWF) Re-Analysis (ERA-40) data (Uppala et al. 2005). The different weather variables were elevation- and bias-corrected using CRU data. Precipitation data were bias corrected using monthly Global Precipitation Climatology Centre (GPCC) precipitation totals (Schneider et al. 2008) and gauge-catch corrections were applied separately for rainfall and snowfall. More information can be found in Weedon et al. (2011). Precipitation (rainfall and snowfall) data from the WFD were used for identification of meteorological drought.

As our study focused on hydrological drought at the global scale, we have used time series of natural total runoff (sum of surface runoff and subsurface runoff, i.e., all water discharged from a single grid cell). Total runoff was chosen because this is most relevant for water resources. All models provide output on a daily time step for the period 1963–2001, following five years of model spinup. The simulated daily data are often highly fluctuating, while hydrological droughts develop over months and years. Therefore, the daily data have been aggregated to monthly time scales for analysis. The ensemble median was calculated from the monthly total runoff time series of all models.

3. Drought analysis

a. Temporal drought identification

To derive drought from time series of total runoff and precipitation for each grid cell, we follow the combined drought identification method, as presented by van Huijgevoort et al. (2012). This method combines the characteristics of the threshold level method (TLM; Yevjevich 1967; Hisdal et al. 2004) and the consecutive dry period method (CDPM; Vincent and Mekis 2006; Groisman and Knight 2008; Deni and Jemain 2009). This combination led to a robust drought indicator for all climates (including regions with frequent periods of zero runoff). The method allows a drought in periods with runoff/precipitation to continue in a following period without runoff/precipitation. For detailed information, the reader is referred to van Huijgevoort et al. (2012).

The 20th percentile (Q20) was used as the threshold in this study. The Q20 is defined as the value that is equaled or exceeded 80% of the time. This means anomalies are identified in each grid cell regardless of the magnitude of runoff/precipitation. The Q20 value was selected in order to be consistent with other global- and large-scale studies (e.g., Corzo Perez et al. 2011; Sheffield et al. 2009; Andreadis et al. 2005). Since this is a rather high threshold value, less extreme events are also identified compared to, for example, a threshold of Q5.

Meteorological drought events have been identified from the monthly precipitation data (1-month data) and for time series with a backward-moving average of a different number of months (3-, 6-, and 9-month data). From the hydrological drought analysis, drought characteristics, such as the number of droughts and their average duration, were derived for each model and the ensemble median at grid cell scale. Since the focus of this paper is not to compare individual models but to assess the potential of using a model ensemble for drought analysis, we use the following relative measure of variability between the model results, the intermodel spread:

$$\text{spread} = (C_{85} - C_{15})/C_{50}, \tag{1}$$

where C is the value of a certain drought characteristic from all models for a grid cell. By taking the 85th and 15th percentiles, the most extreme values in each grid cell (i.e., two most extreme models) were omitted. The spread was calculated for each identified drought characteristic for each grid cell. The spread does not include the absolute values of the runoff, and hence, a complementary diagnostic is required to analyze impacts on local water resources directly. The drought characteristics and spread were visualized in a bivariate color map with the methodology introduced by Teuling

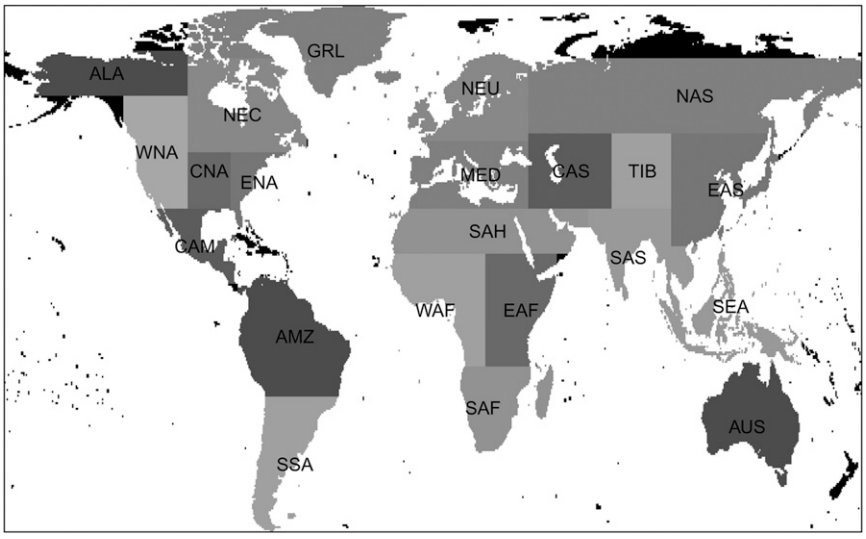

FIG. 1. Location of regions (see Table 2) across the globe as derived from Giorgi and Francisco (2000) and as adapted by Sheffield and Wood (2007).

et al. (2011), which enables plotting of two variables on the same map using a two-dimensional color scale.

In addition to mapping global drought characteristics, time series of area in drought for certain regions were also examined. The regions, which are defined by Giorgi and Francisco (2000) and adapted by Sheffield and Wood (2007), were used to explore model results in more detail at the regional scale (Fig. 1). An overview with full names of the regions is given in Table 2. For these time series of the area in drought, the model variability is shown by the model range. The model range was calculated from all individual model results by excluding the models with the minimum and maximum percentages of area in drought for each region at each time step. Synchronicity in drought between these regions was evaluated with a hierarchical cluster analysis by complete linkage based on the Euclidean distance matrix for time series of the percentages of area in drought derived from the model ensemble median (Hastie et al. 2001). To emphasize the larger drought events in the cluster analysis, percentages below 20% were set to zero in the time series used for the cluster analysis.

b. Spatial drought identification

Simulated drought events generally encompass large regions. Therefore, a flexible method is needed that is able to allocate individual 0.5° grid cells to a given drought cluster. Andreadis et al. (2005) applied a recursion-based approach to link neighboring cells, which are identified to be in drought, into a cluster. Even though this method is easy to implement, recursion-based approaches are generally computationally inefficient and time consuming. A more efficient approach to connect individual cells that experience hydrological drought into a cluster of cells is to apply a component-labeling algorithm (Rosenfeld 1970; Suzuki et al. 2003; Chang et al. 2004). In the current paper, we used a contour-tracing technique (Chang et al. 2004; Wagenknecht 2007) to identify the outer boundaries of a given cluster. Next, cells belonging to the inner regions of a drought cluster are found by applying a connected component-labeling approach (Suzuki et al. 2003; He et al. 2009; Wu et al. 2009). The combination of these two techniques results in a double-pass segmentation algorithm, which is generally assumed to be computationally efficient (He et al. 2009).

TABLE 2. Full names and abbreviations of the regions (see Fig. 1) used in this study (Giorgi and Francisco 2000).

Region	Abbreviation
Alaska	ALA
Northeastern Canada	NEC
Western North America	WNA
Central North America	CNA
Eastern North America	ENA
Central America	CAM
Amazon	AMZ
Southern South America	SSA
Northern Europe	NEU
Northern Asia	NAS
Mediterranean	MED
Central Asia	CAS
Tibetan Plateau	TIB
East Asia	EAS
Southern Asia	SAS
Southeast Asia	SEA
Australia	AUS
Western Africa	WAF
Eastern Africa	EAF
Southern Africa	SAF

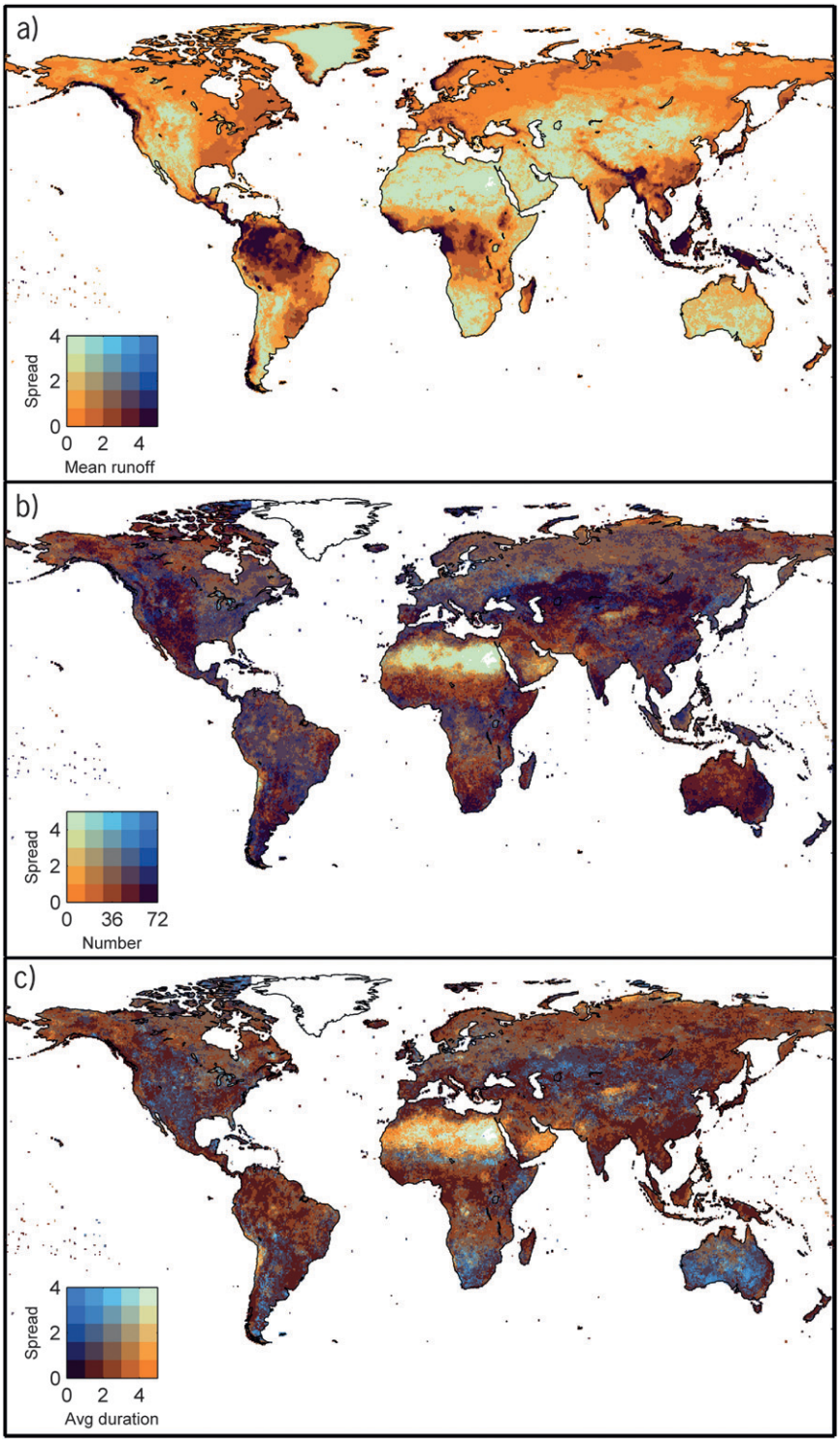

FIG. 2. Drought characteristics and fractional spread in model results [Eq. (1)] for each grid cell: (a) mean runoff (mm day^{-1}), (b) number of droughts, and (c) average duration (months).

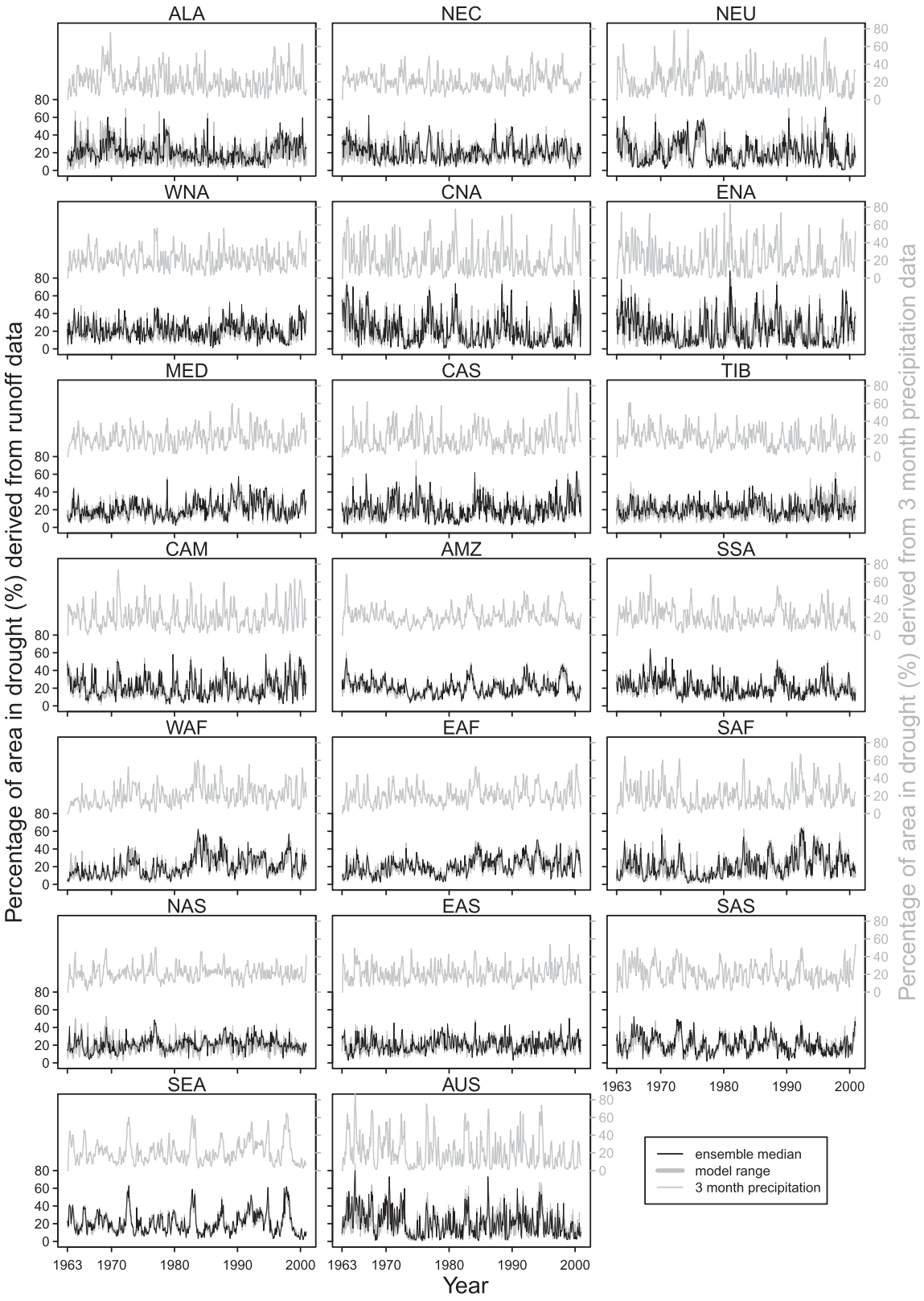

FIG. 3. Fraction in drought for each region derived from precipitation (3-month data), fraction in drought derived from runoff for the ensemble median, and the range of fraction in drought derived from runoff for all models.

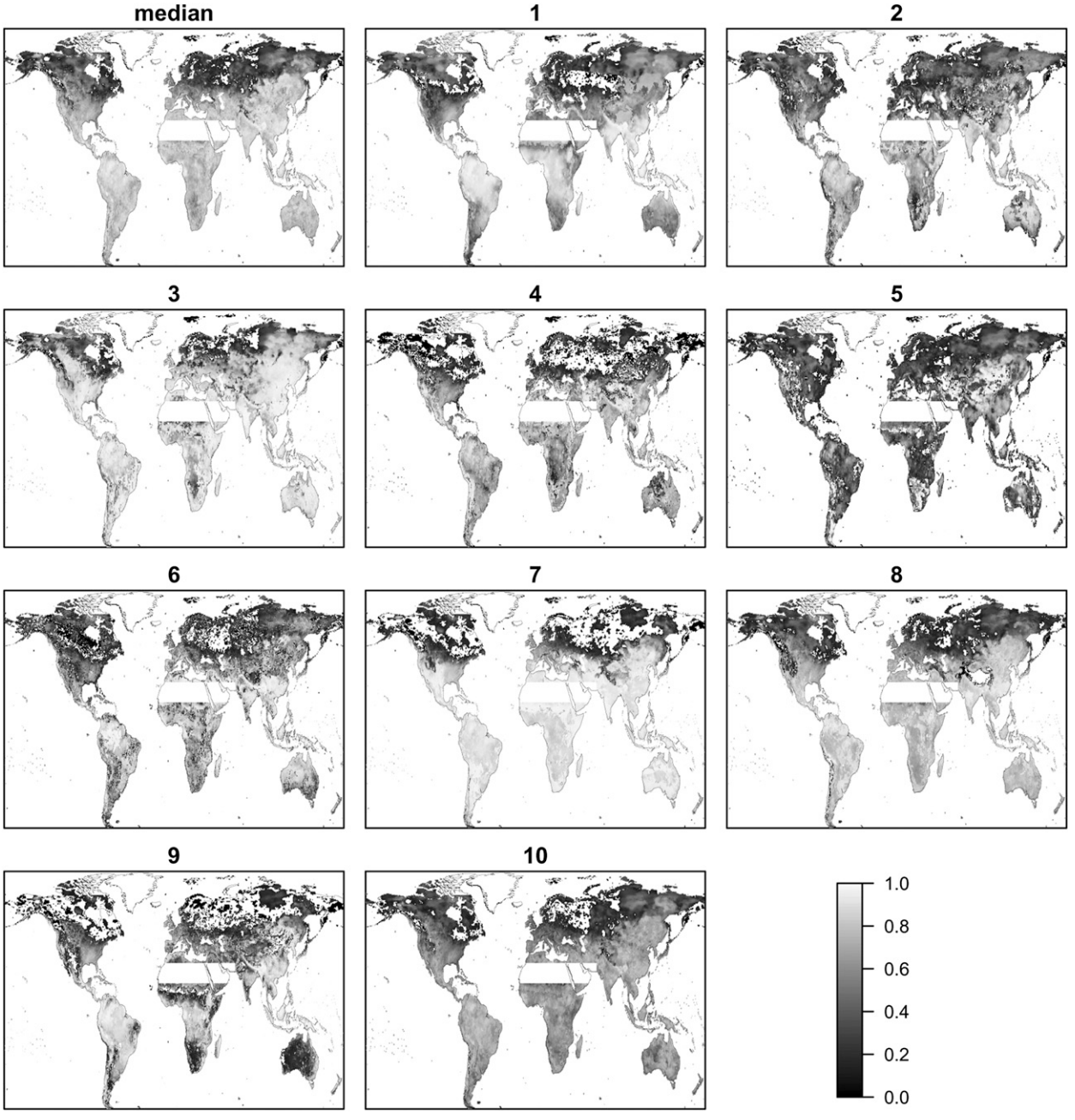

FIG. 4. Correlation between runoff and precipitation (1-month data) in each grid cell for the ensemble median and the individual models (1–10). Greenland and the Sahara region are excluded because of small runoff during the entire period in these areas. Only correlations significantly different from zero at the 95% level using a standard two-sided test are shown, and negative significant correlation values, in this case caused by a continuous snow cover of several months, have been set to zero.

To focus only on major spatial drought events, an areal threshold was implemented (Andreadis et al. 2005; Tallaksen et al. 2009; Sheffield et al. 2009). The areal threshold for a spatial cluster was set to 25 grid cells (approximately 77 275 km^2 around 0° latitude, 62 500 km^2 around 36° latitude, and 26 100 km^2 around 70° latitude).

4. Results

a. Global drought characteristics

For each grid cell, drought characteristics (total number of droughts and average drought duration) have been derived from the runoff time series over the period

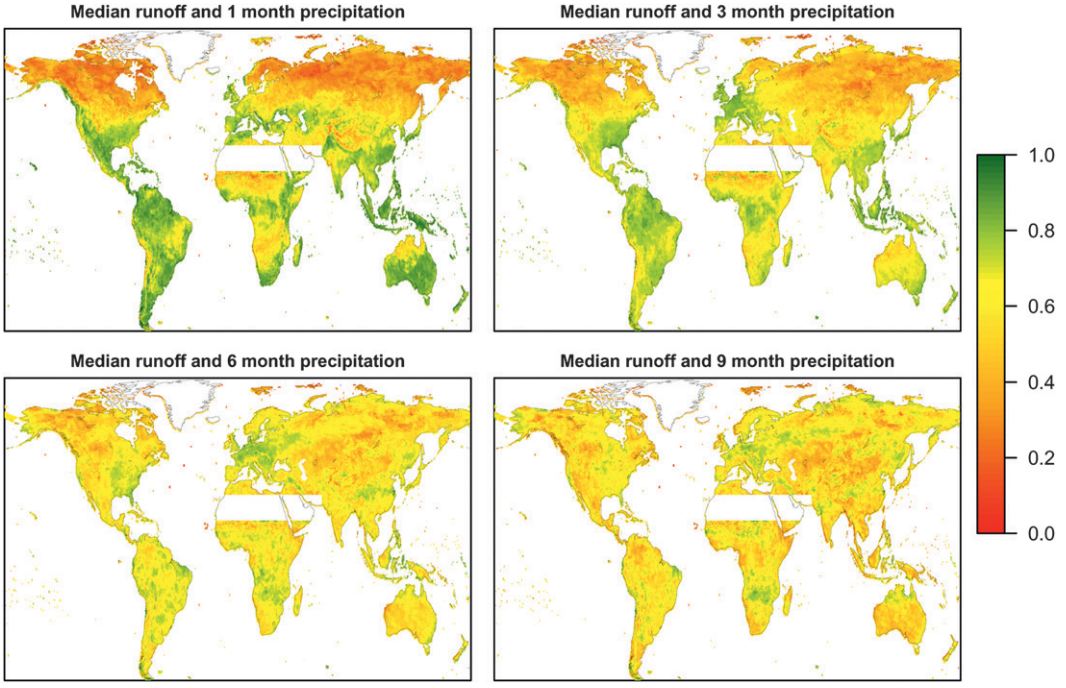

FIG. 5. Correspondence between meteorological drought and runoff drought expressed as the correlation between percentiles determined from the modeled ensemble median runoff and percentiles derived from precipitation data with different aggregation periods (1, 3, 6, and 9 months) in each grid cell. Only correlations significantly different from zero at the 95% level using a standard two-sided test are shown. Greenland and the Sahara region are excluded because of small runoff during the entire period in these areas.

1963–2000. In Fig. 2 the mean runoff and values of the drought characteristics from the ensemble median and spread [Eq. (1)] are illustrated. Regions with the highest spread in mean runoff were the very dry regions (e.g., Sahara) and Greenland (Fig. 2a). The smallest spread occurred in tropical regions (e.g., the Amazon and Southeast Asia), which had high mean runoff values. In most parts of Europe, northern Asia, and the eastern United States, the spread was small as well. Since most models do not include a glacier scheme (Haddeland et al. 2011), the results for Greenland were excluded from further analysis.

Even though considerable differences in runoff values existed (Fig. 2a), the overall patterns of the various drought characteristics were consistent among the models. The largest spread between models in the number of droughts (Fig. 2b) occurred in the (very) dry regions (e.g., Sahara) of the globe. In other regions, the spread was relatively small. For example, all models agreed on a relatively large number of droughts in regions with high runoff (e.g., the Amazon) because, in these areas, runoff exhibits a large variability and therefore often crosses the threshold. Areas with low runoff generally tend to have a smaller number of droughts (e.g., areas adjacent to the Sahara). Striking is the large number of droughts in vast parts of Australia, which was not expected, since runoff was low in these areas as well. This may be caused by the fast reaction of runoff to precipitation in most models in this region. Australia received rainfall, albeit small amounts, more regularly compared to other dry areas, such as the Sahara and its surroundings. These small rainfall amounts led to runoff because of the fast reaction and thus ended hydrological drought events immediately, which decreased drought duration and increased the number of droughts. The same process occurred in other semiarid regions, for example, areas in southwestern United States.

The employed definition of drought (section 3a) implies a negative correlation between the number of droughts and their average duration. This leads to short durations in areas with large runoff variability and long durations when only a few drought events occur (Fig. 2c). Because of this negative correlation, the pattern in the model spread of the average drought duration was similar to the pattern in the spread for the number of droughts.

b. Temporal development of drought

1) RELATION BETWEEN METEOROLOGICAL AND RUNOFF DROUGHT

In the rest of the study, the Sahara region, in addition to Greenland, was not considered because there the

TABLE 3. Correlation between the time series of percentage of area in drought from the ensemble median for the different regions.

	ALA	NEC	NEU	WNA	CNA	ENA	MED	CAS	TIB	CAM
NEC	0.05									
NEU	0.03	0.15								
WNA	0.03	0.11	0.04							
CNA	0.01	0.18	0.13	0.33						
ENA	0.01	0.06	−0.08	0.04	0.44					
MED	−0.15	0.01	−0.09	0.04	−0.15	−0.02				
CAS	0.10	−0.11	−0.01	0.02	0.03	0.06	0.02			
TIB	0.05	−0.14	−0.08	−0.16	−0.15	0.04	−0.10	0.29		
CAM	0.05	−0.08	0.03	0.11	0.13	−0.12	−0.12	0.14	0.03	
AMZ	−0.01	0.16	0.00	−0.14	0.00	0.10	−0.12	−0.22	−0.09	−0.02
SSA	0.06	0.09	0.02	0.09	0.13	0.03	−0.02	0.00	−0.06	−0.02
WAF	−0.16	−0.02	−0.09	−0.11	−0.33	−0.11	0.24	0.04	0.09	−0.07
EAF	−0.11	−0.07	−0.07	−0.03	−0.19	0.00	0.24	0.22	0.15	0.08
SAF	−0.06	0.05	−0.08	0.01	−0.15	0.02	0.17	−0.06	−0.05	−0.09
NAS	−0.16	0.12	0.25	0.14	−0.04	−0.01	−0.02	−0.07	0.00	0.03
EAS	0.10	−0.06	−0.08	−0.05	0.01	0.01	−0.21	0.03	0.20	0.02
SAS	−0.05	0.03	−0.10	−0.09	−0.08	0.08	−0.15	−0.02	0.02	0.06
SEA	−0.16	0.08	−0.04	−0.19	−0.15	−0.08	−0.07	−0.27	0.05	0.00
AUS	−0.01	0.06	0.06	−0.04	0.07	0.05	−0.11	−0.09	−0.06	0.00

models showed large differences and the drought analysis was very difficult, even with the combined method, because of small runoff during the entire period (average annual runoff values of less than 1 mm yr^{-1}). Within each of the remaining regions, the percentage area in drought for each month (Fig. 3) was calculated from the models, from the ensemble median, and from the precipitation data (3-month data). For each month, the model range was determined by excluding the models with the minimum and maximum percentages. The models showed rather small differences in many regions, that is, a small range. Exceptions were Alaska, northern Europe, central North America, eastern North America, southern Africa, and Australia, for which the overall range between the models was largest. The differences in range across the regions were consistent with the patterns in the spread of the drought characteristics and mean runoff (section 4a). Regions with a large runoff variability (e.g., Southeast Asia and the Amazon region) had a small intermodel range in drought percentage. Droughts in these regions are very much controlled by the fast runoff response of almost all models to precipitation. The drought events in both precipitation and runoff occur almost simultaneously in these regions. This fast reaction of the models to precipitation is also shown in Fig. 4, which gives the correlation between monthly precipitation and total runoff time series in each grid cell for all models. Negative correlation values occurring in cold regions, caused by a continuous snow cover of several months, have been set to zero (Fig. 4). Some models reacted faster than others to precipitation in large parts of the world, especially in the Southern Hemisphere, where we found large differences. In general, correlations for all models were lowest in snow-dominated regions, as would be expected. The ensemble median showed relatively high correlations in the Southern Hemisphere, regions around the equator, and South Asia.

To analyze the differences between meteorological drought and runoff drought, correlations between the meteorological drought (time series of percentiles) and runoff drought in the ensemble median (time series of percentiles) were calculated for each grid cell as well (Fig. 5). The meteorological droughts were determined for precipitation aggregated over different periods at 1, 3, 6, and 9 months (section 3a). The correlations showed a clear spatial pattern across the globe, which was similar for the different aggregation periods. Regions with high runoff values showed high correlations, and colder and drier regions gave low correlations. This indicates that the large-scale models add information to the signal derived from the precipitation and that runoff drought cannot directly be determined from precipitation data in global drought analyses when a constant aggregation period is used.

2) SYNCHRONICITY OF DROUGHTS AT GLOBAL SCALE

Since drought events often affect large areas, a single event can occur in several regions simultaneously. Teleconnections may exist for multiple regions, for example, in regions influenced by the El Niño–Southern Oscillation (ENSO) phenomenon (Ropelewski and Halpert 1987). ENSO has a large influence on the occurrence of drought at large scales in both precipitation (e.g., Ropelewski and

TABLE 3. (*Extended*)

CAM	AMZ	SSA	WAF	EAF	SAF	NAS	EAS	SAS	SEA
−0.02									
−0.02	−0.13								
−0.07	0.12	−0.32							
0.08	−0.10	−0.21	0.50						
−0.09	0.27	−0.16	0.26	0.17					
0.03	−0.05	−0.05	0.12	0.17	0.03				
0.02	−0.10	−0.06	−0.08	−0.02	−0.13	−0.01			
0.06	0.10	−0.10	−0.02	0.03	0.08	0.06	0.04		
0.00	0.41	−0.24	0.16	−0.08	0.13	0.05	0.01	0.23	
0.00	0.21	0.03	−0.10	−0.10	0.06	−0.04	−0.10	0.12	0.23

Halpert 1987) and streamflow (e.g., Chiew and McMahon 2002). For the investigation of synchronicity of drought events across the different regions caused by large-scale climate drivers, two different measures were used. First, a hierarchical cluster analysis was applied to identify similarities between the regions. Second, the correlations between the time series of the percentage of area in drought for all regions have been determined (Table 3). The median runoff results showed a larger synchronicity between regions influenced by the ENSO phenomenon and neighboring areas, whereas for other regions no clear pattern was found. Neighboring regions often showed higher correlations (Table 3), for example, central North America with western (0.33) and eastern (0.44) North America and western Africa with eastern Africa (0.50). The cluster analysis also showed similarities in several neighboring regions, for example, regions in Africa, North America, and Asia (Fig. 6). However, there were some unexpected positions of regions in the tree resulting from the cluster analysis (Fig. 6), for example, the western North America, Central America, and Alaska regions. This could be caused by the choices made for the cluster analysis, like the 20% minimum for the percentage of area in drought per region or the use of Euclidean distance (section 3a). The relatively low correlations and similarities between the regions could also cause difficulties in determining homogeneous clusters.

Drought events linked to ENSO were most clearly identified in strong El Niño years (the warm phase of ENSO): 1966, 1972, 1983, 1992, and 1998 (e.g., Smith and Sardeshmukh 2000; Wolter and Timlin 2011). In these years, the regions mainly affected were Australia, Southeast Asia, the Amazon, southern Asia, and southern Africa (Fig. 3), which is consistent with the regions influenced by ENSO mentioned by Vicente-Serrano et al. (2011). These regions showed relatively high correlations in the percentage of area in drought (Table 3), for example Southeast Asia with the Amazon region (0.41). Drought events in these El Niño years were caused by lack of precipitation and strongly linked to the timing of the meteorological droughts (Fig. 3). The same regions, except southern Africa, also showed similarities in the cluster analysis (Fig. 6). Regions affected by

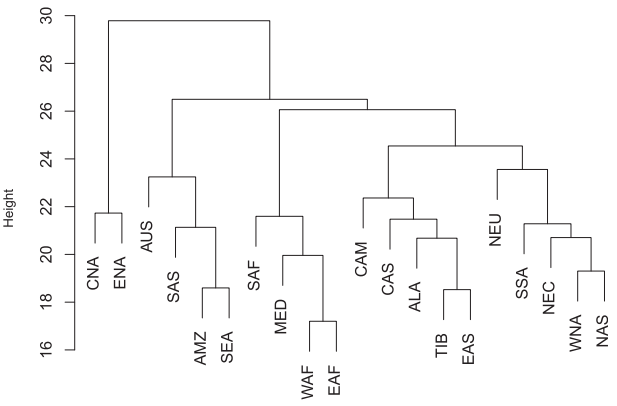

FIG. 6. Hierarchical cluster analysis by complete linkage of time series percentages area in drought (minimum area taken as 20%) derived from the modeled ensemble median runoff, using Euclidean distance matrix, for all regions across the globe. Height is a measure of the dissimilarity between the time series based on the Euclidean distance and is expressed as percentage of area in drought per time step.

La Niña, the southern United States and northern Mexico (central North America and western North America region), southern Russia and eastern Europe (northern Asia, central Asia, and northern Europe regions) and parts of southern South America, often showed negative correlations with the regions affected by El Niño (Table 3), as was expected, for example, southern South America with Southeast Asia (−0.24). Overall, the connection between drought events and La Niña and the synchronicity between the regions were not as strong as for El Niño. This can be explained by the relatively small areas that are affected by La Niña, as compared to the size of the regions used in this study (Fig. 1).

c. *Spatiotemporal development of two major historical drought events*

Two examples of severe drought events have been selected to analyze the spatiotemporal evolution of drought in runoff and precipitation, namely, the mid-1980s drought in Africa and the 1976 drought in Europe. The spatial extent was investigated at continental scale, since these droughts were observed across different regions in Africa and Europe (section 4b).

1) 1980s DROUGHT EVENT IN THE SAHEL

Figures 7a–d show the spatial distributions of the drought in Africa for three different months, derived from the precipitation data (1- and 3-month data), from the runoff of each model and from the ensemble median. The precipitation deficit causing the drought event was clearly identified in the precipitation data both for the 1-month (Fig. 7a) and 3-month data (Fig. 7b), although the spatial extent differed. The spatial extent of the runoff drought event identified by the ensemble median (Fig. 7d) largely resembled the extents found in the precipitation, but disparities were found that indicated the difference between meteorological and hydrological drought caused by the models. All models identified drought somewhere in Africa for all 3 months; however, the spatial extent differed considerably between models (Fig. 7c). The area where at least one model predicted drought (61.1% of total area for October 1983) was much larger than the area for which all models agreed (6.1% of total area), demonstrating the difficulty of drawing any specific conclusion based on a single global model only (Fig. 7c). In this study, the maximum area in drought for all of Africa during this drought event was found at the end of 1983 and again in August 1984. According to Sheffield et al. (2009), this event spread over Africa and reached its maximum extent earlier, namely, in April 1983. Although this timing is different, the spatial extents of the drought over Africa in April 1983 and August 1984 found in the ensemble median were similar to the extents indicated by Sheffield et al. (2009). Differences could be caused by the use of a different drought identification method, which mainly affects dry areas; the use of multiple models instead of a single model; or identification of droughts in different variables (runoff versus soil moisture).

The temporal distribution for the years 1981–86 of the percentage of area in drought for the western Africa region (WAF) determined from precipitation (1- and 3-month data), the ensemble median, and the individual models is given in Figs. 7e and 7f. These time series show the difference between drought in runoff and in precipitation regarding the timing and extent of the event (Fig. 7f). The drought identified in 1-month precipitation data was less extreme and shorter than the drought in 3-month precipitation data. The ensemble median identified droughts more linked to the 3-month precipitation data, indicating the memory and storage included in the models. Even though the models generally showed a fast reaction to precipitation in this region (Fig. 4), a lag and lengthening of the drought event occurred in the propagation to a runoff drought, which indicates that the models add information that cannot be derived from aggregated precipitation deficits. The individual model results showed a variability in the length of the drought event, related to the different model structures determining the response time (Fig. 7e).

2) 1976 DROUGHT EVENT IN EUROPE

The 1976 drought event in Europe (Fig. 8) is illustrated in a similar way as the event in Africa. The spatial distributions of the drought are given in Figs. 8a–d for three different months, derived from the precipitation data (1- and 3-month data), from the runoff of each model, and from the ensemble median. The temporal distribution of the percentage of area in drought for the northern Europe region (NEU) for the years 1974–77 is shown in Figs. 8e and 8f. The meteorological drought determined from monthly precipitation data (Fig. 8a) differed substantially in spatial extent with the drought determined from the 3-month data (Fig. 8b). The latter covered a much larger area of northern Europe in July 1976. The spatial extent of the runoff drought identified with the ensemble median (Fig. 8d) was more in line with the 3-month data, pointing out that the models have a memory of several months when translating the meteorological drought into a hydrological drought. Time series of the percentage of drought for the northern Europe area also show this difference between the drought in precipitation and runoff (Figs. 8e,f). A lengthening of the precipitation event was seen in 1976.

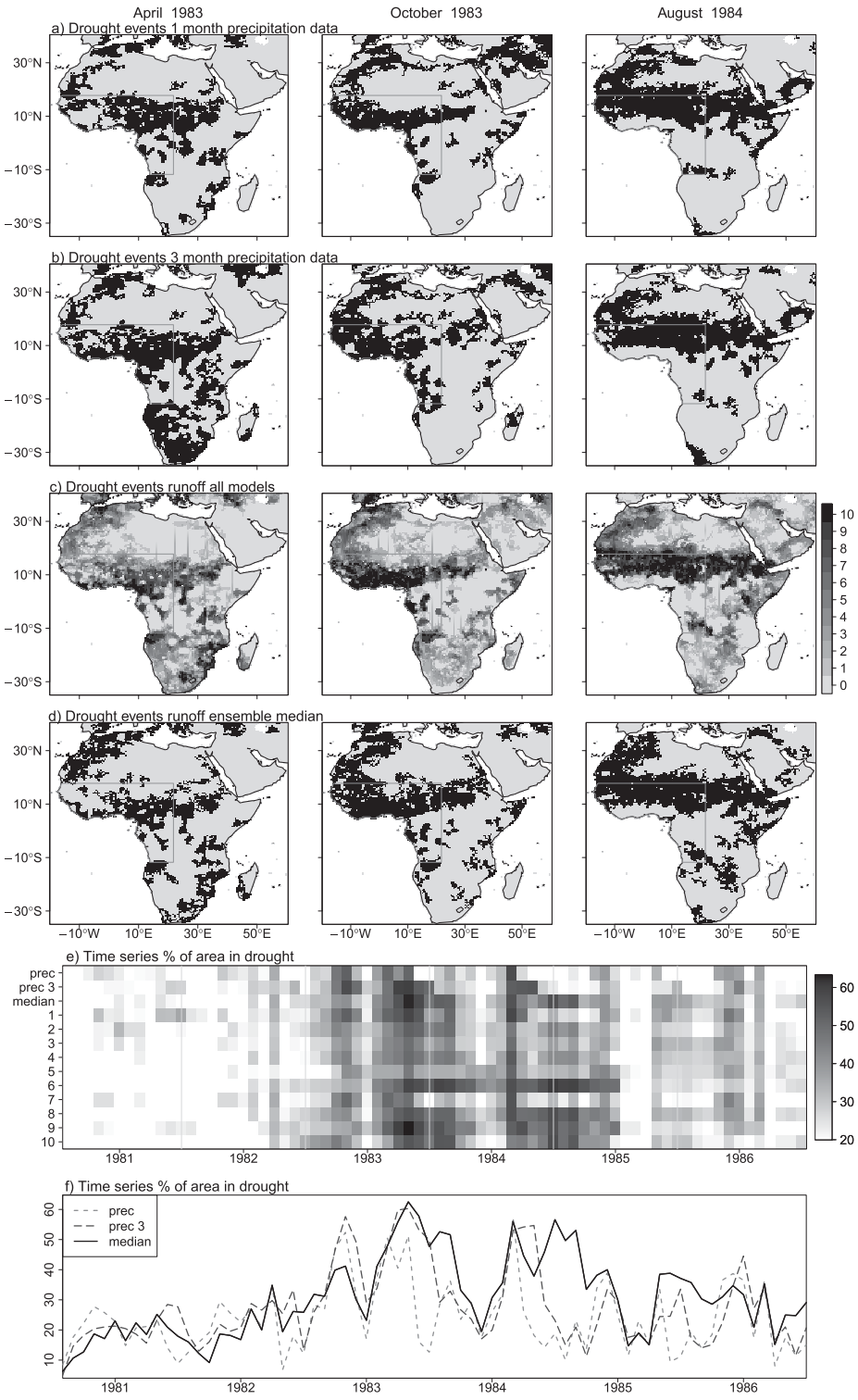

FIG. 7. Spatial distribution of the historical drought event in Africa for (left) April 1983, (middle) October 1983, and (right) August 1984: (a) spatial extent of drought for 1-month precipitation data, (b) spatial extent of drought for 3-month precipitation data, (c) distribution of drought in runoff for all models (10 means all models identify drought, 0 means none of the models identifies drought), (d) spatial extent of drought for ensemble median, (e) temporal development for meteorological drought based on 1- and 3-month data and runoff drought based on ensemble median and individual models (1–10) given as a percentage of area in drought for WAF region [indicated with gray box in (a)–(d)], and (f) percentage of area in drought for meteorological drought based on 1-month (prec) and 3-month (prec 3) data and runoff drought based on ensemble median for WAF region.

The extreme meteorological drought event identified in 1974 was not as extreme in terms of the runoff values (80% of the area in drought for precipitation and 57% of the area in drought regarding runoff from ensemble median). This is also an indication that models reacted less instantaneously to precipitation in this region.

All models started with a drought in Russia and western Europe, which moved to northwestern Europe and ended towards the end of 1976. The spatial extent of the drought event differed substantially among models in all months (in extreme cases the area in drought varied with 30% in the beginning of 1976; Fig. 8e), which also implied that the drought duration produced by each model will differ. Some models interrupted the drought event with lower percentages of area in drought, while others showed a longer continuous event with high percentages (Fig. 8e). Compared to the literature (e.g., Zaidman and Rees 2000; Zaidman et al. 2002; Stahl 2001), the expectation was that all models would give a large area in drought in July 1976. The results presented here, however, show that only for a limited area in Europe all models agreed on July being in drought (5.8% of the total area), although the area in drought for one or more models was much larger (56.5% of the total area had a value of 1 or larger for July 1976; Fig. 8c). In addition, not all models gave the same end date of the drought event (drought recovery). Overall, the median of the models gave qualitatively the same development of the drought event as results of hydrological drought analysis presented in the literature (Zaidman and Rees 2000).

5. Discussion

In this study, we have used a multimodel ensemble to assess whether large-scale models are suitable for drought analysis. A large variability in model results was found, which means the identified drought events can be very different for individual models. The reason for this variability is difficult to determine, since the many different model structures and parameter values for individual cells make it very difficult to understand the differences between models (e.g., Gudmundsson et al. 2012b). Therefore, the focus in this study was not on the individual models, but instead on the ensemble median and variability. The use of multiple models has been quite common in climate studies; however, for impact studies, often only one single hydrological model has been used. With the importance of using multiple impact models now increasingly being appreciated, the latest climate change impact projects, for example, the Inter-Sectoral Impact Model Intercomparison Project (ISI-MIP; www.isi-mip.org), will employ multiple hydrological models. To reduce the uncertainties between models, performance of the models across a range of output variables, such as evaporation, soil moisture storage, groundwater storage, and their covariance, could be investigated. Suitability of different models for different regions in the world could be determined with this kind of analysis, which was beyond the scope of this study. By including additional variables, propagation of drought could be studied in more detail and processes not represented in the models could be identified. Van Loon et al. (2012) have performed such an analysis for several individual grid cells with contrasting climate and concluded that storage and evaporation processes could be improved in the models. Until a perfect model exists for analysis across the globe with, among others, ideal stores and parameters included, the use of multiple models is recommended to account for a range of uncertainty.

The largest spread between the models was found in the dry regions of the world. This is consistent with the results of Haddeland et al. (2011), showing a relatively large spread of simulated runoff in arid and semiarid regions. This can partly be explained by the use of different evapotranspiration and infiltration methods in the models. Since runoff is low in these regions, small differences in evaporation lead to relatively large differences in runoff (Haddeland et al. 2011). Most large-scale models overestimate the runoff in dry regions because of several processes not being included in these models, for example, the transmission loss along the river channel or infiltration and evaporation of surface runoff (Gosling and Arnell 2011; Haddeland et al. 2011).

With respect to the temporal development of drought, relatively large differences among the models were also observed in cold regions (e.g., Alaska and Tibetan Plateau). Other studies, focusing specifically on Europe, have found that model performance in simulating the observed hydrological response is lower in regions with snow influence than in regions without snow (Stahl et al. 2012; Gudmundsson et al. 2012b). This can be explained by the different implementations of snow processes, such as accumulation, sublimation, and melt, and differences in the partitioning of precipitation into rainfall and snowfall between the models (Haddeland et al. 2011).

In general, we found that the ensemble median is capable of identifying the major drought events. Because all models have the same forcing data and major drought events are climate driven, all models capture the occurrence of these events. This suggests that large-scale models could be used for the simulation of major droughts, as previously concluded by Prudhomme et al. (2011), who compared three different large-scale models

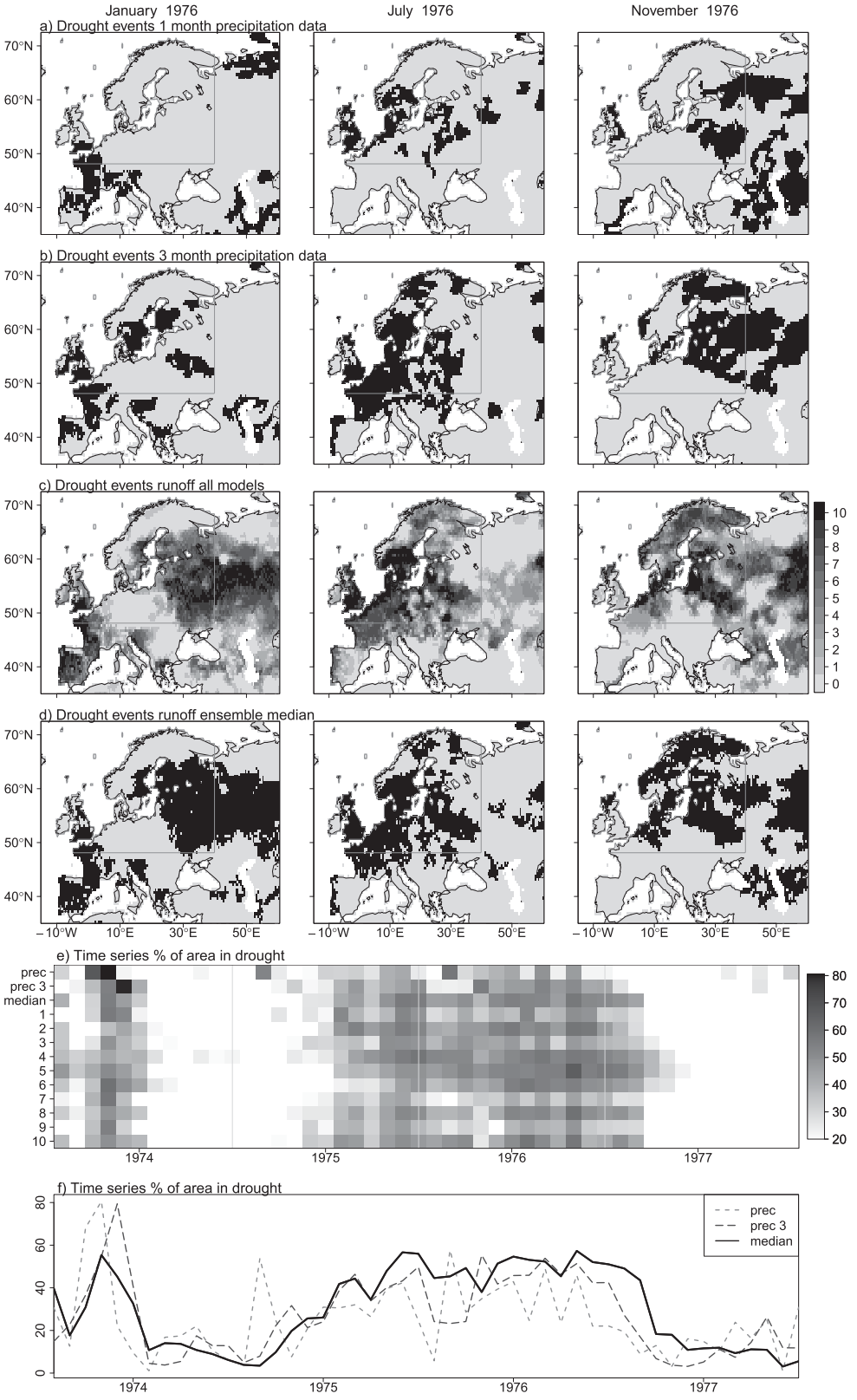

FIG. 8. As in Fig. 7, but for the historical drought event in Europe for (left) January 1976, (middle) July 1976, and (right) November 1976 and the northern Europe region.

for Europe and found that these models are able, to some extent, to simulate low runoff anomalies. However, this study shows that the duration and spatial extent of simulated drought events are less consistent. These drought characteristics depend on catchment characteristics such as hydrogeology (Tallaksen and van Lanen 2004). Some models showed a very fast runoff response to precipitation, implying that simulation of storage-related processes is limited. This leads to deviations in drought events in parts of the world where stores (e.g., groundwater, lakes) play an important role in drought propagation (Van Loon and van Lanen 2012). These results are consistent with the conclusions of Wang et al. (2009), Stahl et al. (2012), and Gudmundsson et al. (2012a). Stahl et al. (2012) noted for areas with groundwater-dominated systems that the nature and magnitude of such complex storages cannot be replicated by the simplified storage schemes used in the current generation of large-scale models. This relatively fast reaction in runoff also explains the lack of multiyear droughts, since generally hydrological droughts ended too soon (e.g., Van Loon et al. 2012).

Even though in this study we made a first step to determine the suitability of large-scale models for hydrological drought analysis, validation of the model output remains difficult because of the lack of observations and the limited number of independent drought studies at the global scale for runoff or streamflow. Global observations of river flow cannot be directly compared with gridded runoff values of the models because this would require a proper routing procedure and because of the scale of the models, would require relatively large river basins (e.g., Haddeland et al. 2011), which are often affected by dams and abstractions.

6. Conclusions

One of the main objectives of this paper was to investigate whether large-scale models are able to reproduce the spatiotemporal development of hydrological drought at the global and continental scale. In the current study, variability (spread and range) between 10 different large-scale models, their ensemble median of runoff, and global precipitation data were used for drought analysis. For all models, a set of general runoff drought characteristics, for example, number and duration per cell, was derived. As expected, all models yielded many short drought events in areas with high runoff and few long drought events in areas with low runoff values. The largest spread was found in very dry areas and very cold areas, and the smallest spread was in areas with high runoff. The differences between the models were caused by the different model structures and parameterizations. Therefore, conclusions on global drought occurrence based on single models vary strongly depending on the model used.

Time series of percentage of area in drought for selected regions across the world led to a similar conclusion, with a large range in model outcomes in cold and dry areas and a small range in high runoff areas. However, simulated drought durations differed substantially between the models. The models showed limitations in identification of multiyear droughts. Because of imperfect simulation of storage-related processes in some models, the runoff reacted very fast to precipitation, and long-term memory effects were lacking in some regions. However, by using a multimodel ensemble, the impact of this problem was alleviated, since some of the models do have larger groundwater storages. The correlation between meteorological drought events and runoff drought events derived from the ensemble median showed a distinct spatial pattern across the globe for several aggregation periods of precipitation. This indicates that at a global scale runoff drought cannot be determined from precipitation data alone using a constant aggregation period. Given the uncertainty caused by the variability among the models, the results presented here clearly encourage the use of multiple global hydrological models instead of one single model.

Overall, when focusing on major drought events, a multimodel ensemble gives new insight into the development of drought in space and time at global and continental scales. Further improvement of large-scale models is possible and will lead to improved ability to simulate hydrological drought events.

Acknowledgments. This research has been financially supported by the EU-FP6 Project WATCH (036946), the EU-FP7 Project IMPRINTS (226555), and the EU-FP7 Project DROUGHT-R&SPI (282769). The research contributes to the program of the Wageningen Institute for Environment and Climate Research (WIMEK-SENSE), and it supports the work of the UNESCO-IHP VII EURO-FRIEND Programme. The authors thank Graham Weedon (UK Met Office) for supplying the WATCH forcing data. We further thank Sandra Gomes (Centro de Geofisica da Universidade de Lisboa, Portugal) and Nathalie Bertrand (Laboratoire de Météorologie Dynamique, France) for providing model results.

REFERENCES

Alcamo, J., P. Döll, T. Henrichs, F. Kaspar, B. Lehner, T. Rösch, and S. Siebert, 2003: Development and testing of the WaterGAP 2 global model of water use and availability. *Hydrol. Sci. J.,* **48,** 317–337, doi:10.1623/hysj.48.3.317.45290.

Andreadis, K. M., E. A. Clark, A. W. Wood, A. F. Hamlet, and D. P. Lettenmaier, 2005: Twentieth-century drought in the

conterminous United States. *J. Hydrometeor.,* **6,** 985–1001, doi:10.1175/JHM450.1.

Arnell, N. W., 1999: A simple water balance model for the simulation of streamflow over a large geographic domain. *J. Hydrol.,* **217,** 314–335, doi:10.1016/S0022-1694(99)00023-2.

Balsamo, G., P. Viterbo, A. Beljaars, B. van den Hurk, M. Hirschi, A. K. Betts, and K. Scipal, 2009: A revised hydrology for the ECMWF model: Verification from field site to terrestrial water storage and impact in the integrated forecast system. *J. Hydrometeor.,* **10,** 623–643, doi:10.1175/2008JHM1068.1.

Best, M. J., and Coauthors, 2011: The Joint UK Land Environment Simulator (JULES), model description—Part 1: Energy and water fluxes. *Geosci. Model Dev.,* **4,** 677–699, doi:10.5194/gmd-4-677-2011.

Bondeau, A., P. C. Smith, S. Zaehle, S. Schaphoff, W. Lucht, W. Cramer, and D. Gerten, 2007: Modelling the role of agriculture for the 20th century global terrestrial carbon balance. *Global Change Biol.,* **13,** 679–706, doi:10.1111/j.1365-2486.2006.01305.x.

Chang, F., C. J. Chen, and C. J. Lu, 2004: A linear-time component-labeling algorithm using contour tracing technique. *Comput. Vision Image Understanding,* **93,** 206–220, doi:10.1016/j.cviu.2003.09.002.

Chiew, F. H. S., and T. A. McMahon, 2002: Global ENSO-streamflow teleconnection, streamflow forecasting and interannual variability. *Hydrol. Sci. J.,* **47,** 505–522, doi:10.1080/02626660209492950.

Clark, D. B., and Coauthors, 2011: The Joint UK Land Environment Simulator (JULES), model description—Part 2: Carbon fluxes and vegetation dynamics. *Geosci. Model Dev.,* **4,** 701–722, doi:10.5194/gmd-4-701-2011.

Corzo Perez, G. A., M. H. J. van Huijgevoort, F. Voß, and H. A. J. van Lanen, 2011: On the spatio-temporal analysis of hydrological droughts from global hydrological models. *Hydrol. Earth Syst. Sci.,* **15,** 2963–2978, doi:10.5194/hess-15-2963-2011.

Dai, A., 2011: Drought under global warming: A review. *Wiley Interdiscip. Rev.: Climate Change,* **2,** 45–65, doi:10.1002/wcc.81.

de Rosnay, P., and J. Polcher, 1998: Modelling root water uptake in a complex land surface scheme coupled to a GCM. *Hydrol. Earth Syst. Sci.,* **2,** 239–255, doi:10.5194/hess-2-239-1998.

Deni, S. M., and A. A. Jemain, 2009: Mixed log series geometric distribution for sequences of dry days. *Atmos. Res.,* **92,** 236–243, doi:10.1016/j.atmosres.2008.10.032.

Fraser, E. D., E. Simelton, M. Termansen, S. N. Gosling, and A. South, 2013: ''Vulnerability hotspots'': Integrating socio-economic and hydrological models to identify where cereal production may decline in the future due to climate change induced drought. *Agric. For. Meteor.,* **170,** 195–205, doi:10.1016/j.agrformet.2012.04.008.

Gao, X., and P. A. Dirmeyer, 2006: A multimodel analysis, validation, and transferability study of global soil wetness products. *J. Hydrometeor.,* **7,** 1218–1236, doi:10.1175/JHM551.1.

Giorgi, F., and R. Francisco, 2000: Uncertainties in regional climate change prediction: a regional analysis of ensemble simulations with the HADCM2 coupled AOGCM. *Climate Dyn.,* **16,** 169–182, doi:10.1007/PL00013733.

Gosling, S. N., and N. W. Arnell, 2011: Simulating current global river runoff with a global hydrological model: Model revisions, validation, and sensitivity analysis. *Hydrol. Processes,* **25,** 1129–1145, doi:10.1002/hyp.7727.

Groisman, P. Ya., and R. W. Knight, 2008: Prolonged dry episodes over the conterminous United States: New tendencies emerging during the last 40 years. *J. Climate,* **21,** 1850–1862, doi:10.1175/2007JCLI2013.1.

Gudmundsson, L., and Coauthors, 2012a: Comparing large-scale hydrological model simulations to observed runoff percentiles in Europe. *J. Hydrometeor.,* **13,** 604–620, doi:10.1175/JHM-D-11-083.1.

——, T. Wagener, L. M. Tallaksen, and K. Engeland, 2012b: Evaluation of nine large-scale hydrological models with respect to the seasonal runoff climatology in Europe. *Water Resour. Res.,* **48,** W11504, doi:10.1029/2011WR010911.

Guo, Z., P. A. Dirmeyer, X. Gao, and M. Zhao, 2007: Improving the quality of simulated soil moisture with a multi-model ensemble approach. *Quart. J. Roy. Meteor. Soc.,* **133,** 731–747, doi:10.1002/qj.48.

Haddeland, I., and Coauthors, 2011: Multi-model estimate of the global terrestrial water balance: Setup and first results. *J. Hydrometeor.,* **12,** 869–884, doi:10.1175/2011JHM1324.1.

Hagemann, S., and L. Dümenil, 1997: A parametrization of the lateral waterflow for the global scale. *Climate Dyn.,* **14,** 17–31, doi:10.1007/s003820050205.

——, and L. D. Gates, 2003: Improving a subgrid runoff parameterization scheme for climate models by the use of high resolution data derived from satellite observations. *Climate Dyn.,* **21,** 349–359, doi:10.1007/s00382-003-0349-x.

Hanasaki, N., S. Kanae, T. Oki, K. Masuda, K. Motoya, N. Shirakawa, Y. Shen, and K. Tanaka, 2008: An integrated model for the assessment of global water resources—Part 1: Model description and input meteorological forcing. *Hydrol. Earth Syst. Sci.,* **12,** 1007–1025, doi:10.5194/hess-12-1007-2008.

Hastie, T., R. Tibshirani, and J. Friedman, 2001: *The Elements of Statistical Learning: Data Mining, Inference, and Prediction.* Springer-Verlag, 533 pp.

He, L., Y. Chao, K. Suzuki, and K. Wu, 2009: Fast connected-component labeling. *Pattern Recognit.,* **42,** 1977–1987, doi:10.1016/j.patcog.2008.10.013.

Hisdal, H., L. M. Tallaksen, B. Clausen, E. Peters, and A. Gustard, 2004: Hydrological drought characteristics. *Hydrological Drought Processes and Estimation Methods for Streamflow and Groundwater,* L. M. Tallaksen and H. A. J. van Lanen, Eds., Developments in Water Science, Vol. 48, Elsevier Science, 139–198.

Koirala, S., 2010: Explicit representation of groundwater process in a global-scale land surface model to improve hydrological predictions. Ph.D. thesis, University of Tokyo, 208 pp.

Meigh, J. R., A. A. McKenzie, and K. J. Sene, 1999: A grid-based approach to water scarcity estimates for eastern and southern Africa. *Water Resour. Manage.,* **13,** 85–115, doi:10.1023/A:1008025703712.

Prudhomme, C., S. Parry, J. Hannaford, D. B. Clark, S. Hagemann, and F. Voss, 2011: How well do large-scale models reproduce regional hydrological extremes in Europe? *J. Hydrometeor.,* **12,** 1181–1204, doi:10.1175/2011JHM1387.1.

Romm, J., 2011: The next dust bowl. *Nature,* **478,** 450–451, doi:10.1038/478450a.

Ropelewski, C. F., and M. S. Halpert, 1987: Global and regional scale precipitation patterns associated with the El Niño/Southern Oscillation. *Mon. Wea. Rev.,* **115,** 1606–1626, doi:10.1175/1520-0493(1987)115<1606:GARSPP>2.0.CO;2.

Rosenfeld, A., 1970: Connectivity in digital pictures. *J. Assoc. Comput. Mach.,* **17,** 146–160, doi:10.1145/321556.321570.

Rost, S., D. Gerten, A. Bondeau, W. Lucht, J. Rohwer, and S. Schaphoff, 2008: Agricultural green and blue water consumption and its influence on the global water system. *Water Resour. Res.,* **44,** W09405, doi:10.1029/2007WR006331.

Schneider, U., T. Fuchs, A. Meyer-Christoffer, and B. Rudolf, 2008: Global Precipitation Analysis Products of the GPCC.

GPCC Rep., 13 pp. [Available online at ftp://ftp.dwd.de/pub/data/gpcc/PDF/GPCC_intro_products_v2011.pdf.]

Seneviratne, S. I., and Coauthors, 2012: Changes in climate extremes and their impacts on the natural physical environment. *Managing the Risks of Extreme Events and Disasters to Advance Climate Change Adaptation,* C. B. Field et al., Eds., Cambridge University Press, 109–230.

Sheffield, J., and E. F. Wood, 2007: Characteristics of global and regional drought, 1950–2000: Analysis of soil moisture data from off-line simulation of the terrestrial hydrologic cycle. *J. Geophys. Res.,* **112,** D17115, doi:10.1029/2006JD008288.

——, K. M. Andreadis, E. F. Wood, and D. P. Lettenmaier, 2009: Global and continental drought in the second half of the twentieth century: Severity-area-duration analysis and temporal variability of large-scale events. *J. Climate,* **22,** 1962–1981, doi:10.1175/2008JCLI2722.1.

Smith, C. A., and P. D. Sardeshmukh, 2000: The effect of ENSO on the intraseasonal variance of surface temperatures in winter. *Int. J. Climatol.,* **20,** 1543–1557, doi:10.1002/1097-0088(20001115)20:13<1543::AID-JOC579>3.0.CO;2-A.

Stahl, K., 2001: Hydrological drought—A study across Europe. Ph.D. thesis, Albert-Ludwigs-Universität Freiburg, 113 pp. [Available online at http://www.hydrology.uni-freiburg.de/publika/FSH-Bd15-Stahl.pdf.]

——, L. M. Tallaksen, J. Hannaford, and H. A. J. van Lanen, 2012: Filling the white space on maps of European runoff trends: estimates from a multi-model ensemble. *Hydrol. Earth Syst. Sci.,* **16,** 2035–2047, doi:10.5194/hess-16-2035-2012.

Suzuki, K., I. Horiba, and N. Sugie, 2003: Linear-time connected-component labeling based on sequential local operations. *Comput. Vision Image Understanding,* **89,** 1–23, doi:10.1016/S1077-3142(02)00030-9.

Takata, K., S. Emori, and T. Watanabe, 2003: Development of the minimal advanced treatments of surface interaction and runoff. *Global Planet. Change,* **38,** 209–222, doi:10.1016/S0921-8181(03)00030-4.

Tallaksen, L. M., and H. A. J. van Lanen, Eds., 2004: *Hydrological Drought: Processes and Estimation Methods for Streamflow and Groundwater*. Developments in Water Science, Vol. 48, Elsevier Science, 579 pp.

——, H. Hisdal, and H. A. J. van Lanen, 2009: Space-time modelling of catchment scale drought characteristics. *J. Hydrol.,* **375,** 363–372, doi:10.1016/j.jhydrol.2009.06.032.

——, K. Stahl, and G. Wong, 2011: Space-time characteristics of large-scale droughts in Europe derived from streamflow observations and WATCH multi-model simulations. WATCH Tech. Rep. 48, 16 pp. [Available online at http://www.eu-watch.org/publications/technical-reports.]

Teuling, A. J., R. Stoeckli, and S. I. Seneviratne, 2011: Bivariate colour maps for visualizing climate data. *Int. J. Climatol.,* **31,** 1408–1412, doi:10.1002/joc.2153.

Uppala, S. M., and Coauthors, 2005: The ERA-40 re-analysis. *Quart. J. Roy. Meteor. Soc.,* **131,** 2961–3012, doi:10.1256/qj.04.176.

van Huijgevoort, M. H. J., P. Hazenberg, H. A. J. van Lanen, and R. Uijlenhoet, 2012: A generic method for hydrological drought identification across different climate regions. *Hydrol. Earth Syst. Sci.,* **16,** 2437–2451, doi:10.5194/hess-16-2437-2012.

Van Loon, A. F., and H. A. J. van Lanen, 2012: A process-based typology of hydrological drought. *Hydrol. Earth Syst. Sci.,* **16,** 1915–1946, doi:10.5194/hess-16-1915-2012.

——, M. H. J. van Huijgevoort, and H. A. J. van Lanen, 2012: Evaluation of drought propagation in an ensemble mean of large-scale hydrological models. *Hydrol. Earth Syst. Sci.,* **16,** 4057–4078, doi:10.5194/hess-16-4057-2012.

Vicente-Serrano, S. M., J. I. Lopez-Moreno, L. Gimeno, R. Nieto, E. Moran-Tejeda, J. Lorenzo-Lacruz, S. Begueria, and C. Azorin-Molina, 2011: A multiscalar global evaluation of the impact of ENSO on droughts. *J. Geophys. Res.,* **116,** D20109, doi:10.1029/2011JD016039.

Vincent, L. A., and E. Mekis, 2006: Changes in daily and extreme temperature and precipitation indices for Canada over the twentieth century. *Atmos.–Ocean,* **44,** 177–193, doi:10.3137/ao.440205.

Wagenknecht, G., 2007: A contour tracing and coding algorithm for generating 2D contour codes from 3D classified objects. *Pattern Recognit.,* **40,** 1294–1306, doi:10.1016/j.patcog.2006.09.003.

Wang, A., T. J. Bohn, S. P. Mahanama, R. D. Koster, and D. P. Lettenmaier, 2009: Multimodel ensemble reconstruction of drought over the continental United States. *J. Climate,* **22,** 2694–2712, doi:10.1175/2008JCLI2586.1.

——, D. P. Lettenmaier, and J. Sheffield, 2011: Soil moisture drought in China, 1950–2006. *J. Climate,* **24,** 3257–3271, doi:10.1175/2011JCLI3733.1.

Weedon, G. P., and Coauthors, 2011: Creation of the WATCH forcing data and its use to assess global and regional reference crop evaporation over land during the twentieth century. *J. Hydrometeor.,* **12,** 823–848, doi:10.1175/2011JHM1369.1.

Wilhite, D., Ed., 2000: *Drought: A Global Assessment.* Routledge, 752 pp.

Wolter, K., and M. S. Timlin, 2011: El Niño/Southern Oscillation behaviour since 1871 as diagnosed in an extended multivariate ENSO index (MEI.ext). *Int. J. Climatol.,* **31,** 1074–1087, doi:10.1002/joc.2336.

Wu, K., E. Otoo, and K. Suzuki, 2009: Optimizing two-pass connected-component labeling algorithms. *Pattern Anal. Appl.,* **12,** 117–135, doi:10.1007/s10044-008-0109-y.

Yevjevich, V., 1967: An objective approach to definition and investigations of continental hydrologic droughts. Hydrology Paper 23, Colorado State University, Fort Collins, CO, 19 pp.

Zaidman, M. D., and H. G. Rees, 2000: Spatial patterns of streamflow drought in Western Europe 1960–1995. ARIDE Tech. Rep. 8, Centre for Ecology and Hydrology, Wallingford, UK, 57 pp. [Available online at http://www.hydrology.uni-freiburg.de/forsch/aride/navigation/publications/pdfs/aride-techrep8.pdf.]

——, ——, and A. R. Young, 2002: Spatio-temporal development of streamflow droughts in north-west Europe. *Hydrol. Earth Syst. Sci.,* **6** , 733–751, doi:10.5194/hess-6-733-2002.